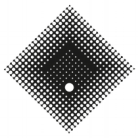
VICTORIA UNIVERSITY
MELBOURNE AUSTRALIA

Nonlinear analysis of rectangular concrete-filled double steel tubular short columns incorporating local buckling

This is the Accepted version of the following publication

Ahmed, Mizan, Liang, Qing, Patel, Vipulkumar Ishvarbhai and Hadi, Muhammad NS (2018) Nonlinear analysis of rectangular concrete-filled double steel tubular short columns incorporating local buckling. Engineering Structures, 175. 13 - 26. ISSN 0141-0296

The publisher's official version can be found at https://www.sciencedirect.com/science/article/pii/S014102961831229X
Note that access to this version may require subscription.

Downloaded from VU Research Repository https://vuir.vu.edu.au/37683/

Ahmed, M., Liang, Q. Q., Patel, V. I. and Hadi, M. N. S. (2018). Nonlinear analysis of rectangular concrete-filled double steel tubular short columns incorporating local buckling. *Engineering Structures*, 175: 13-26.

Nonlinear analysis of rectangular concrete-filled double steel tubular short columns incorporating local-buckling

Mizan Ahmed[a], Qing Quan Liang[a,*], Vipulkumar Ishvarbhai Patel[b], Muhammad N. S. Hadi[c]

[a] *College of Engineering and Science, Victoria University, PO Box 14428, Melbourne, VIC 8001, Australia*
[b] *School of Engineering and Mathematical Sciences, La Trobe University, Bendigo, VIC 3552, Australia*
[c] *School of Civil, Mining and Environmental Engineering, University of Wollongong, Wollongong, NSW 2522, Australia*

ABSTRACT

Rectangular concrete-filled double steel tubular (CFDST) columns with inner circular steel tube possess higher structural performance than conventional concrete-filled steel tubular (CFST) columns. However, the local buckling of the outer steel tube of thin-walled rectangular CFDST columns has not been accounted for in the existing fiber element models and design codes that may overestimate the column ultimate axial strengths. This paper describes a computationally efficient fiber-based modeling technique developed for determining the behavior of concentrically-loaded rectangular CFDST short columns including the local buckling effects of the external steel tube and the confinement offered by the internal circular steel tube. The effective width concept is used to simulate the post-local buckling of the outer steel tube. Comparative studies are undertaken to verify the fiber-based model with the relevant test results. The computational model is then employed to investigate the axial load-strain responses of rectangular CFDST short columns with various key design variables. A design equation is developed for computing the ultimate axial loads of short rectangular CFDST columns and compared with design methods given in several international design codes. It is shown that the

*Corresponding author. Tel.: 61 3 9919 4134.
E-mail address: Qing.Liang@vu.edu.au (Q. Q. Liang)

fiber-based modeling technique and the proposed design model predict well the structural performance of short CFDST columns.

Keywords: Concrete-filled double steel tubes; nonlinear analysis; local buckling; post-local buckling.

1. Introduction

The rectangular concrete-filled double steel tubular (CFDST) column is a high performance composite column, which is constructed by an outer rectangular steel tube and an inner circular steel tube filled with concrete as depicted in Fig. 1. Experiments conducted by Knowles and Park [1], Tomii et al. [2], Schneider [3] and Sakino et al. [4] indicated that the rectangular or square steel tube provided little confinement to the filled concrete while the circular steel tube offered a significant confinement to the concrete infill. The addition of a circular steel tube to the rectangular concrete-filled steel tubular (CFST) column remarkably improves the column structural performance. The circular steel tube provides confinement to the core concrete, which increases the strength and ductility of the core concrete and thereby improves the ultimate axial loads, stiffness, ductility, shear-resistance and fire-resistance of CFDST columns. The concrete within the inner circular steel tube not only prevents the local buckling of the inner steel tube but also increases the overall buckling strength and fire-resistance of the inner hollow steel tube. Therefore, thin-walled rectangular CFDST columns are utilized in high-rise composite steel-concrete buildings, industrial buildings and bridges to support heavy loads. The CFDST columns are characterized by the outward local-buckling of the external rectangular steel tube. However, the local buckling effects have not been incorporated in the fiber-based analysis models for thin-walled CFDST columns and in international design codes including Eurocode 4 [5], ACI 318-11 [6], AISC 360-16 [7] and AIJ [8]. A fiber element simulation technique

considering the local buckling effects and concrete confinement is much needed for accurately predicting the axial load-strain responses of rectangular CFDST columns with thin-walled sections.

Computational and experimental investigations on the responses of circular short CFDST columns subjected to axial loading have been undertaken by researchers, such as Peng et al. [9], Hassanein et al. [10], Wan and Zha [11], Xiong et al. [12], and Ekmekyapar and Al-Eliwi [13]. These studies showed that the core concrete was confined by both the inner and outer circular steel tubes, which increased both the ductility and capacity of circular CFDST columns. Ahmed et al. [14] proposed confinement models for the core concrete in short CFDST circular columns based on available test results while the confinement model presented by Hu et al. [15] was adopted to compute the maximum compressive strength of the concrete between the two tubes. The fiber technique implementing these confinement models was shown to capture well the behavior of circular CFDST short columns.

Relatively limited investigations on the behavior of square CFDST columns under static loading were conducted by researchers [16-20]. Lu and Zhao [16] presented a numerical method for computing the load-deflection relationships of eccentrically-loaded square slender CFDST columns with various width-to-thickness, loading eccentricity and column slenderness ratios. Pei [18] performed experimental investigations on short and slender square CFDST columns subjected to axial and eccentric loading and used the finite element software ANSYS to analyze square CFDST short columns. The effects of the inner circular tube with various thicknesses, diameters and steel yield stresses on the performance of CFDST columns were examined. The 23 square short CFDST columns under axial compressive loads were tested to failure by Qian et al. [19]. The experimental results indicated that the local buckling of the square steel tube

occurred outwardly while the sandwiched concrete near the buckled regions crushed. However, these square CFDST columns still could withstand about 70% of the ultimate axial loads and had the ultimate axial strains ranging from 0.09 to 0.11. The finite element software ABAQUS was utilized by Qian et al. [19] to analyze short square CFDST columns including local buckling effects. Wang et al. [20] undertook tests on 12 square cold-formed thin-walled CFDST short columns with stiffeners under axial compression. It was reported that the failure mode of all CFDST columns was the outward local buckling of the external square steel tube. The outer steel tube at the stiffeners buckled locally outward because the sandwiched concrete crushed and the stiffeners buckled. No local buckling of the inner circular steel tube was observed so that the core concrete was effectively confined by the internal tube, which improved the column ultimate load and ductility. The finite element software ABAQUS was employed by Wang et al. [20] to study the behavior of short CFDST columns.

It should be noted that at the early loading stage, the inner circular steel tube does not provide confinement to the core concrete because the Poisson's ratio of the concrete is less than that of the steel. When the axial compressive stress in concrete is greater than its unconfined compressive strength, the sandwiched concrete crushes and separates from the inner steel tube. Under this high axial compressive stress, the core concrete expanses and eventually inserts a lateral pressure on the inner steel tube so that the inner circular steel tube confines the core concrete. In the numerical analysis, the confinement effect is considered in the stress-strain model for concrete in circular steel tubes when the axial compressive stress in the concrete is greater than its unconfined compressive strength as discussed by Liang [21].

The dynamic and impact responses of CFDST columns and double-skin concrete-filled steel tubular (DCFST) columns have been studied in recent years. Han et al. [22] developed a fiber

element model for determining the cyclic behavior of square and circular DCFST beam-columns with inner circular tubes. Simple models were proposed that compute the moment-curvature and lateral load-deflection responses of DCFST beam-columns under cyclic lateral loads. The seismic performance of high-strength square CFDST columns with various geometric parameters and axial force levels were experimentally investigated by Qian et al. [23]. It was observed that the sandwiched and core concrete crushed and the outer square steel tube buckled locally outward. Wang et al. [24] employed ABAQUS software to quantify the effects of impact height as well as geometric and material properties on the behavior of circular DCFST columns under lateral impact. They reported that the hollow ratio had a significant effect on the dynamic resistance of DCFST columns, which should account for the dynamic increase factor when the confinement factor is greater than 1.03. The blast resistance of square DCFST columns made of high performance steel-fiber reinforced concrete was studied experimentally and numerically by Zhang et al. [25]. The experimental results showed that square DCFST columns could resist a large blast load without failure. Aghdamy et al. [26] utilized the finite element software LS-DYNA to investigate the effects of load-related parameters on the behavior of circular DCFST columns under lateral impact. Large-scale tests and numerical analyses on the flexural behavior of square DCFST members under blast loads were conducted by Ritchie et al. [27]. Their study indicated that increasing the width of the inner steel tube increased the ultimate moment capacity of DCFST columns and the width and thickness of the outer tube had a significant effect on the ductility of DCFST columns.

The local buckling of the external steel tube is one of the main failure modes associated with rectangular CFDST short columns with inner circular steel tube. The local buckling of thin steel plates restrained by concrete was studied previously by researchers [28-33]. Liang and Uy [31] derived effective width models for calculating the post-local buckling strength of steel plates in

rectangular CFST columns based on finite element analyses. Liang et al. [32] utilized these effective width models in the inelastic analysis of rectangular short CFST columns. Liang et al. [33] also investigated the local and post-local buckling strengths of steel tube walls of rectangular CFST columns under biaxial loads and developed expressions for determining initial local and post-local buckling strengths of clamped steel plates. The expressions were implemented in the fiber based models to include local buckling in the inelastic simulations of CFST columns subjected to biaxial loads by Liang [34, 35].

Although the local buckling of the external rectangular steel tube in CFDST columns could be considered in the finite element analysis using commercial programs, the nonlinear inelastic finite element analysis of CFDST columns is highly time consuming and expensive. This paper presents a computationally efficient fiber-based modeling technique for the simulation of rectangular CFDST short columns including the effects of the progressive local and post-local buckling of the outer rectangular steel tube. The fiber-based analysis technique incorporates the confinement to the core concrete offered by the inner circular steel tube. The model validation is performed by comparing the predicted ultimate axial strength and load-strain relationships with the corresponding test results. The developed computer program is then used to evaluate the influences of important variables on the ultimate load and behavior of short CFDST columns. A design formula is developed for rectangular short CFDST columns considering the concrete confinement and local buckling and verified by independent test results as well as design codes.

2. Fiber element modeling

2.1. Efficiency of the fiber element technique

Although the commercial finite element software such as ABAQUS and ANSYS can be used to develop 3D models for the nonlinear analysis of CFDST columns, the 3D finite element models are tedious to be built and expensive. As pointed out by Liang [36], many 3D elements must be used to divide the column along its length in the finite element modeling so that the model contains many degrees of freedom. The interactions between the concrete and steel tubes are simulated using contract elements. In addition to the development time of the 3D model for each CFDST column, its computational cost is very high compared to the fiber element model that does not require the discretization of the column along its length. The finite element model of Specimen I-CSCFT4 given in Table 1 was developed using ABAQUS and is shown in Fig. 2. The time for creating the 3D finite element model was 13 minutes while its computational time was 31 minutes. The mesh of the fiber element model is presented in Fig. 3. The user does not need to create the fiber element model for each CFDST column but needs to input the data of the column. The data input time for Specimen I-CSCFT4 was 15 seconds while the computational time of the fiber element model was 10 seconds. The total time for creating and analyzing the finite element model was 2640 seconds while the total time for creating and analyzing the fiber element model was only 25 seconds. This demonstrates that the fiber element technique significantly saves the development and computational time of the composite column model compared to the finite element method. The verification of the fiber element model is given in Section 3.

2.2. Section discretization and stress calculation

The numerical model is formulated based on the fiber element method in this paper. In the fiber analysis, the cross-section of a CFDST column is discretized into small fibers which represent either the steel or concrete [34, 37]. The stress of each fiber is computed using the

material uniaxial stress-strain constitutive laws for steel or concrete and integrated over the area of the entire cross-section to compute the stress resultants such as the axial load and moment. Figure 3 shows the typical fiber mesh of the column cross-section. In the computer program, the outer steel tube thickness is divided into layers as specified by the user and the steel tube wall is automatically discretized along the width on the basis of the layer size [34]. The fiber discretization of the sandwiched concrete is undertaken using a mesh generation algorithm proposed by Persson and Strang [38]. The algorithm was derived based on simple mechanical analogy where the nodal locations are solved for equilibrium in 2-D truss structures using the linear force-displacement relationship and reset the topology by the Delaunay algorithm [38]**.** A non-uniform desire edge length function results in finer resolution for the fibers close to the circle as shown in Fig. 3. The discretization of the inner circular tube and concrete core is similar to the conventional CFST column [39].

2.3. Constitutive laws of steels

The stress-strain constitutive laws for structural steels employed in the fiber model are shown in Fig. 4. The idealized stress-strain model for structural steels suggested by Liang [34] is adopted for strain up to the onset of strain-hardening. Beyond this point, the expression given by Mander [40] is used to model the strain hardening behavior. A reduction in the yield stress due to the biaxial stresses on the steel tubes of CFDST columns under compression is considered in the stress-strain model. The stress within the strain range of $0.9\varepsilon_{sy} < \varepsilon_s \le \varepsilon_{st}$ is determined by the following equation derived by Liang [34]:

$$\sigma_s = f_{sy}\left(\frac{\varepsilon_s - 0.9\varepsilon_{sy}}{\varepsilon_{st} - 0.9\varepsilon_{sy}}\right)^{\frac{1}{45}} \quad (1)$$

in which σ_s represents the longitudinal steel stress and ε_s is the corresponding strain; f_{sy} and ε_{sy} denote the yield strength and strain respectively; and ε_{st} stands for the strain at the onset of strain hardening which is specified as 0.005 in the nonlinear analysis.

The stress within the strain range of $\varepsilon_{st} < \varepsilon_s \le \varepsilon_{su}$ is calculated using the expressions developed by Mander [40] as follows:

$$\sigma_s = f_{su} - \left(\frac{\varepsilon_{su} - \varepsilon_s}{\varepsilon_{su} - \varepsilon_{st}} \right)^n (f_{su} - f_{sy}) \tag{2}$$

$$n = E_{st} \left(\frac{\varepsilon_{su} - \varepsilon_{st}}{f_{su} - f_{sy}} \right) \tag{3}$$

where ε_{su} is the ultimate strain taken as 0.2, E_{st} is the modulus at the onset of strain hardening taken as $0.02E_s$, and f_{su} denotes the tensile strength of steel.

2.4. Initial local buckling of the external steel tube

The rectangular CFDST column made of an outer non-compact or slender steel section is susceptible to local buckling. When the applied axial load attains the initial local buckling stress of the steel plate, the plate undergoes local buckling. Liang et al. [33] derived expressions for computing the initial local-buckling strength of clamped steel plates as part of the CFST column based on the finite element analysis results. Local geometric imperfection and residual stresses of steel plates resulted from the induction of heating and welding during the production were considered in the formulation of these equations. The equation given by Liang et al. [33] is used

to estimate the initial local buckling stress of the outer steel tube wall subjected to uniform edge compressive stresses, and is written as

$$\frac{\sigma_{cr}}{f_{syo}} = 0.5507 + 0.005132\left(\frac{b}{t_o}\right) - 9.869\times10^{-5}\left(\frac{b}{t_o}\right)^2 + 1.198\times10^{-7}\left(\frac{b}{t_o}\right)^3 \quad (4)$$

where σ_{cr} and f_{syo} are the initial local buckling stress and yield strength of the outer steel tube wall with imperfections respectively, and t_o is the thickness of the outer steel tube.

2.5. Post-local buckling of the outer steel tube

After the onset of initial local buckling, the progressive post-local buckling behavior of steel plate under increasing applied load can be described by the method of stress redistribution. The stresses are redistributed to the unloaded edge strips from the central area of the steel plate which heavily buckles and carries lower stresses compared to the edge strips. The post-local buckling strength of the steel plate can be calculated using the effective width illustrated in Fig. 5. The following effective width formula derived by Liang et al. [33] for the steel tube walls of CFST columns subjected to uniform compression is adopted in the present study:

$$\frac{b_e}{b} = 0.5554 + 0.02038\left(\frac{b}{t_o}\right) - 3.944\times10^{-4}\left(\frac{b}{t_o}\right)^2 + 1.921\times10^{-6}\left(\frac{b}{t_o}\right)^3 \quad (5)$$

where b and b_e are the clear width and the effective width of the steel tube wall, respectively. At the ultimate strength state, the maximum ineffective width $b_{ne,\max}$ of the steel tube wall is computed by

$$b_{ne,\max} = b - b_e \tag{6}$$

The ineffective width b_{ne} can be calculated by linear interpolation depending on the stress level of the steel fiber using the following expression [32]:

$$b_{ne} = \left(\frac{\sigma_s - \sigma_{cr}}{f_{syo} - \sigma_{cr}} \right) b_{ne,\max} \tag{7}$$

In the computation, the steel fiber stresses are firstly calculated by the stress-strain laws and are checked against the criterial local buckling stress for possible local buckling. For steel tube walls having a b/t_o ratio greater than 30, if $\sigma_s > \sigma_{cr}$, the ineffective width of the steel plate is computed and the fiber stresses within this area are assigned to zero until the maximum $b_{ne,\max}$ is attained.

2.6. Constitutive laws of concrete

Confinement models have been proposed for determining the compressive strength of concrete in CFST columns [4, 15, 39, 41-43]. For rectangular CFDST columns with inner circular tube, it is assumed that the outer rectangular steel tube does not induce confinement to the core concrete as well as the sandwiched concrete and the internal circular steel tube offers confinement to the core concrete. Therefore, the stress-strain model given by Liang [34] for concrete in rectangular CFST columns can be applied to the sandwiched concrete while the stress-strain model provided by Liang and Fragomeni [39] for concrete in circular CFST columns can be used for the core concrete in the inner steel tube in CFDST columns. The idealized stress-strain laws of concrete in a rectangular CFDST column presented in Fig. 6 are

adopted in the present model. The stress-strain model consists of two Parts: (1) the ascending part and (2) the descending parabolic part. The stress-strain relationships suggested by Liang [34] are used to simulate the ascending branch while the descending branch is described by the equations proposed by Lim and Ozbakkaloglu [44]. The compressive strength of confined concrete ($f_{cc}^{'}$) and its corresponding strain ($\varepsilon_{cc}^{'}$) are calculated by the equations provided by Lim and Ozbakkaloglu [44]. However, the lateral confining pressure model proposed by Liang and Fragomeni [39] is adopted to determine the lateral pressures on the core concrete as it has been well established and verified by experimental data. Moreover, the post-peak behavior of the concrete is modeled by the residual strength and the concrete degradation factor β_c proposed in the present study based on experimental results on CFDST columns.

The ascending branch of the stress-strain curve is defined by the following formula presented by Mander et al. [45]:

$$\sigma_c = \frac{f_{cc}^{'}(\varepsilon_c / \varepsilon_{cc}^{'})\lambda}{(\varepsilon_c / \varepsilon_{cc}^{'})^{\lambda} + \lambda - 1} \qquad (0 \le \varepsilon_c \le \varepsilon_{cc}^{'}) \tag{8}$$

in which σ_c stands for the longitudinal concrete stress, ε_c is the corresponding strain and λ is calculated as

$$\lambda = \frac{E_c \varepsilon_{cc}^{'}}{E_c \varepsilon_{cc}^{'} - f_{cc}^{'}} \tag{9}$$

where E_c represents the Young's modulus of concrete. The original equation for E_c proposed by Lim and Ozbakkaloglu [44] is modified to consider the effect of column size using the factor γ_c as

$$E_c = 4400\sqrt{\gamma_c f_c'} \quad \text{(MPa)} \tag{10}$$

where $f_c^{'}$ is the compressive strength of the concrete cylinder, and the reduction factor γ_c is computed as $1.85D_c^{-0.135}$ suggested by Liang [34] and is limited to $0.85 \le \gamma_c \le 1.0$. The parameter D_c is the diameter of the circular concrete core and for rectangular sections, it is taken as the larger of $(B_o - 2t_o)$ and $(D_o - 2t_o)$.

The descending parabolic branch of the stress-strain curve is determined by the following expression given by Lim and Ozbakkaloglu [44]

$$\sigma_c = f_{cc}^{'} - \frac{f_{cc}^{'} - f_{cr}}{\left[1 + \left(\dfrac{\varepsilon_c - \varepsilon_{cc}^{'}}{\varepsilon_{ci} - \varepsilon_{cc}^{'}}\right)^{-2}\right]} \qquad (\varepsilon_{cc}^{'} < \varepsilon_c) \tag{11}$$

where $f_{cc}^{'}$ and $\varepsilon_{cc}^{'}$ represent the compressive strength and corresponding strain of the confined concrete, respectively. Lim and Ozbakkaloglu [44] proposed expressions to calculate $f_{cc}^{'}$ and $\varepsilon_{cc}^{'}$ based on extensive test results. Their expressions are modified here to consider the effect of column size using the factor γ_c as follows:

$$f_{cc}^{'}=\gamma_c f_c^{'}+5.2(\gamma_c f_c^{'})^{0.91}\left(\frac{f_{rp}}{\gamma_c f_c^{'}}\right)^{a} \qquad \text{where} \quad a=(\gamma_c f_c^{'})^{-0.06} \tag{12}$$

$$\varepsilon_{cc}^{'}=\varepsilon_c^{'}+0.045\left(\frac{f_{rp}}{\gamma_c f_c^{'}}\right)^{1.15} \tag{13}$$

$$\varepsilon_c^{'}=\frac{(\gamma_c f_c^{'})^{0.225}}{1000} \tag{14}$$

in which f_{rp} denotes the lateral pressure applied by the steel tube on the concrete.

The lateral pressure f_{rp} on the sandwiched concrete between the two steel tubes is zero so that its compressive strength is determined as $f_{cc}^{'}=\gamma_c f_c^{'}$. For the core concrete in a CFDST column, the lateral confining pressure is calculated using the confinement model developed by Liang and Fragomeni [39] for concrete in circular CFST columns, which is expressed by

$$f_{rpi}=\begin{cases}0.7(v_e-v_s)\dfrac{2t_i}{D_i-2t_i}\,f_{syi} & \text{for } \dfrac{D_i}{t_i}\le 47\\[2ex] (0.006241-0.0000357\dfrac{D_i}{t_i})\,f_{syi} & \text{for } 47<\dfrac{D_i}{t_i}\le 150\end{cases} \tag{15}$$

where D_i and t_i represent the diameter and thickness of the inner circular tube, respectively; v_e and v_s are the Poisson's ratios of the steel tube with and without concrete infill, respectively. In the fiber model, the Poisson's ratio $v_s=0.5$ is used and v_e is provided by Tang et al. [46] as

$$v_e=0.2312+0.3582v_e^{'}-0.1524\left(\frac{\gamma_c f_c^{'}}{f_{syi}}\right)+4.843v_e^{'}\left(\frac{\gamma_c f_c^{'}}{f_{syi}}\right)-9.169\left(\frac{\gamma_c f_c^{'}}{f_{syi}}\right)^2 \tag{16}$$

$$v_e^{'} = 0.881\times10^{-6}\left(\frac{D_i}{t_i}\right)^3 - 2.58\times10^{-4}\left(\frac{D_i}{t_i}\right)^2 + 1.953\times10^{-2}\left(\frac{D_i}{t_i}\right) + 0.4011 \tag{17}$$

In the stress-strain curve shown in Fig. 6, f_{cr} is the residual concrete strength. The expression proposed by Lim and Ozbakkaloglu [44] is utilized to calculate the residual strength of the core concrete within the inner circular steel tube, which is written as

$$f_{cr} = \begin{cases} f_{cc}^{'} & \text{for } \dfrac{D_i}{t_i} \le 40 \\ 1.6 f_{cc}^{'}\left(\dfrac{f_{rp}^{0.24}}{(\gamma_c f_c^{'})^{0.32}}\right) \text{ and } f_{cr} \le f_{cc}^{'} - 0.15(\gamma_c f_c^{'}) & \text{for } 40 < \dfrac{D_i}{t_i} \le 150 \end{cases} \tag{18}$$

The residual concrete strength of the sandwiched concrete can be calculated as $f_{cr} = \beta_c f_c^{'}$, where β_c is the concrete strength degradation factor, which is related to the width-to-thickness ratio (B_s / t_o) of CFDST columns, where B_s is taken as the larger of B_o and D_o of the outer steel tube. Previous research on rectangular CFST columns with $B_s / t_o \le 24$ is found to be less susceptible to local buckling and recommended β_c value as 1.0 [34]. Based on the previous study on rectangular CFST columns [34] and by interpreting the test results of CFDST short columns as shown in Fig. 7, the factor β_c for CFDST columns with $B_s / t_o > 24$ is proposed as

$$\beta_c = \begin{cases} 1 - \dfrac{(B_s / t_o - 24)}{15} & \text{for } 24 < \dfrac{B_s}{t_o} \le 33 \\ 0.000062\left(\dfrac{B_s}{t_o}\right)^2 - 0.011225\left(\dfrac{B_s}{t_o}\right) + 0.705288 & \text{for } 33 < \dfrac{B_s}{t_o} \le 100 \end{cases} \tag{19}$$

In Eq. (11), ε_{ci} is the strain corresponding to the inflection point that determines the shape of the descending curve. For the sandwiched concrete, ε_{ci} is taken as 0.007. For the core concrete, the expression developed by Lim and Ozbakkaloglu [44] and modified using the factor γ_c is used to calculate ε_{ci} as follows:

$$\varepsilon_{ci} = 2.8\varepsilon_{cc}^{'}\left(\frac{f_{cr}}{f_{cc}^{'}}\right)\left(\gamma_c f_c^{'}\right)^{-0.12} + 10\varepsilon_{cc}^{'}\left(1-\frac{f_{cr}}{f_{cc}^{'}}\right)\left(\gamma_c f_c^{'}\right)^{-0.47} \tag{20}$$

2.7. Ductility index

The ductility index measures the ductility of a CFDST column and is defined as

$$PI_{sd} = \frac{\varepsilon_u}{\varepsilon_y} \tag{21}$$

where ε_u denotes the axial strain when the axial load drops to 90% of its ultimate load in the post-peak regime or the ultimate strain in the case where column shows ascending stress-strain curve followed by reaching the yielding point. The yield strain (ε_y) is taken as $\varepsilon_{0.75}/0.75$, where $\varepsilon_{0.75}$ stands for the corresponding strain when axial load obtains 75% of its ultimate load.

3. Comparisons of computations with experimental results

The numerical model is validated by comparisons of the predicted ultimate loads and load-strain responses of axially loaded rectangular CFDST short columns with corresponding test

data provided by Qian et al. [19], Wang et al. [20] and Pei [18]. The test data of the specimens is given in Table 1. In the numerical analysis, the compressive strength of concrete cylinder $f_c^{'}$ was taken as 85% of the concrete cube strength as suggested by Oehlers and Bradford [47]. In the analysis of the Specimens tested by Wang et al. [20], the local buckling of the outer tube was considered by ignoring the effect of the stiffeners, but the areas of the stiffeners were included. Table 1 shows the computed ultimate axial strengths $\left(P_{u,num}\right)$ and experimentally measured strengths $\left(P_{u,\exp}\right)$ of CFDST columns. It appears that the fiber-based technique captures well the ultimate loads of axially loaded rectangular CFDST short columns. The mean of $P_{u,num} / P_{u,\exp}$ is 0.95 with the corresponding standard deviation of 0.04. However, the predicted ultimate axial loads of Specimens III-CSCFT3 to III-CSCFT7 are below or equal to 90% of the experimental results. This is likely caused by the uncertainty of the actual strength of concrete in these specimens. The model is further validated by comparing the measured axial load-strain responses of square CFDST short columns with computer solutions in Figs. 8 to 10. Good agreement between the experimental and predicted responses is obtained. The computed initial stiffness of the columns is in excellent agreement with the measured one. Furthermore, the comparison shows that the proposed fiber-based model predicts the column residual strengths with reasonable accuracy.

4. Parametric study

The performance of rectangular CFDST columns with inner circular tube is influenced by both material and geometric properties of the columns. The numerical model proposed was used to examine the influences of key design available on the performance of CFDST columns. The material and geometric properties of CFDST columns considered are listed in Table 2. The corresponding tensile strengths of steel tubes with the yield stresses of 250, 350, 450 and 520

MPa were taken as 320, 430, 520 and 620 MPa, respectively. The Young's modulus of 200 GPa was used for all steel tubes.

4.1. Effects of inner circular tube

The influences of inner circular tube on the ultimate axial capacity and post-peak behavior of CFDST columns were investigated by the fiber-based model. The fiber element analyses of CFDST Column C2 and the reference CFST Column C1 given in Table 2 were performed. The two columns had the same cross-section and the same cross-sectional steel area. Figure 11 illustrates that the ultimate load-carrying capacity of the Column C2 is increased by 10.43% due to the internal circular steel tube compared with that of Column C1. In addition, the circular internal steel tube increases the residual strength of the Column C2 by 32% in comparison with that of Column C1 without an inner steel tube. Moreover, the ductility index increases from 1.75 to 2.23 by strengthening the CFST column (C1) with an inner circular tube. As depicted in Fig. 11, the addition of an inner circular steel tube to the CFST column does not have a notable influence on the column initial stiffness.

The effects of diameter and thickness of the inner circular steel tube on the behavior of CFDST short columns were investigated by the fiber modeling technique. Fiber analyses on Columns C2-C5 in Table 2 with diameters ranging from 150 to 300 mm were conducted. The computed axial load-strain responses of the columns are presented in Fig. 12. It is seen that increasing the diameter of the inner steel tube considerably increases the ultimate axial loads of CFDST short columns. The column ultimate load is found to increase by 15.2% by increasing the diameter of the inner steel tube from 150 mm to 300 mm. It is noted that the larger of the diameter of the inner steel tube, the larger of the cross-sectional steel area, concrete area confined by the circular

steel tube and thus the higher of the column ultimate axial strength. Columns C2 and C6-C8 presented in Table 2 had thickness of the inner steel tube varied from 6.0 to 15.0 mm. Figure 13 demonstrates the effects of the thickness of the inner steel tube on the behavior of CFDST columns. It appears that the column ultimate axial strength is markedly increased by increasing the thickness of the inner steel tube. When the thickness of the inner steel tube increases from 6.0 to 7.5, 10 and 15 mm, the increase in the column ultimate axial load is 6.0%, 9.8% and 16.5%, respectively. This is attributed to the increase in the steel area and the confinement to the core concrete.

4.2. Effects of local buckling

Column C9 in Table 2 was analyzed to determine the influences of local buckling on the axial load-strain performance of short CFDST columns. The D_o / t_o ratio of the column was 99.5, which was so large that the local buckling of the external square steel tube under compression occurred. Fiber analyses on the column were undertaken by taking into consideration the local buckling of the external steel tube and ignoring its effect, respectively. Figure 14 demonstrates that local buckling reduces the column ultimate axial load. When local buckling is not considered, the ultimate load of the CFDST short column is overestimated by 7.9%. Figure 14 shows that the residual strength of the CFDST short column is also overestimated by ignoring local buckling effects.

4.3. Effects of concrete strength

To investigate the influences of concrete strengths on the performance of CFDST short column, the Columns C10-C21 filled with concrete with various compressive strengths in Table 2 were

analyzed by using the fiber modeling technique. The only variable considered was the concrete compressive strength. Three cases were considered: (1) the strength of the sandwiched and core concrete was the same; (2) the core concrete strength was varied; and (3) the strength of the sandwiched concrete was varied. For the first case, the concrete strength was increased from 35 MPa to 50, 70 and 90 MPa. The axial load capacity of the square CFDST columns increases with increasing the concrete strength as illustrated in Fig. 15. However, the ductility of the columns decreases with increasing the concrete strength. Changing the concrete strength from 35 MPa to 90 MPa results in a decrease in the ductility index from 4.5 to 2.85 as shown in Fig. 16. For the second case, the concrete strength of the sandwiched concrete was 50 MPa while the strength of the core concrete was increased from 35 MPa to 50, 70 and 90 MPa. The computed axial load-strain relationships of short columns as a function of concrete strength are presented in Fig. 17. The column ultimate axial load is not significantly affected by the core concrete strength. For the third case, the strength of the core concrete was 50 MPa while the strength of the sandwiched concrete was increased from 35 MPa to 50, 70 and 90 MPa. As shown in Fig. 18, the column ultimate strength is increased significantly by increasing the strength of the sandwiched concrete. The column made of concrete with 90 MPa has a ductility index of 2.81 while it is 4.75 for the column with 35 MPa sandwiched concrete.

4.4. Effects of steel yield strength

The computational model was used to study the influences of the yield strength of the steel tubes on the performance of CFDST columns. Two groups of short columns were investigated for this purpose. In the first case, the yield strength (f_{syo}) of the outer steel tubes of Columns C22-C25 in Table 2 was varied while the yield stress of the internal tube f_{syi} was fixed to 350 MPa. In the second case, the yield strength of the internal steel tubes of Columns C26-C29 in

Table 2 was changed while the yield stress of the outer tubes was 350 MPa. The predicted load-strain curves of these columns are presented in Figs. 19 and 20. It is observed that the column ultimate axial strength is increased considerably by increasing the yield stresses of either the outer or the inner steel tube. When the steel yield stress of the inner steel tube is changed from 250 MPa to 350, 450 and 520 MPa, the column ultimate axial load increases by 5.7%, 10.2% and 13.1%, respectively. On the contrary, by increasing f_{syo} from 250 MPa to 350, 450 and 520 MPa, the ultimate load of CFDST columns increases by 6.05%, 11.4% and 14.8%, respectively.

4.5. Effects of B_o / D_o ratio

The width-to-depth ratio (B_o / D_o) influences the performance of CFDST columns. Columns C30-C33 in Table 2 had different B_o / D_o ratios but had an identical inner tube. When the B_o / D_o ratio is increased from 0.5 to 0.75, 1.25 and 1.5, the column ultimate strength increases by 25.5%, 49.8% and 56.8%, respectively. This is due to the fact that the area of the sandwiched concrete is increased by increasing the B_o / D_o ratio and the sandwiched concrete carries most of the load. The load-strain curves of Columns C30-C33 are presented in Fig. 21. It is demonstrated that the lager the B_o / D_o ratio, the poor the ductility. The residual strength of Column C32 with B_o / D_o ratio of 1.25 is only about 48.3% of the column ultimate strength.

5. Proposed design model

In this study, a simple design formula was developed for computing the ultimate axial strength of rectangular CFDST short columns as follows:

$$P_{u,des} = f_{syo}A_{soe} + \gamma_{si} f_{syi}A_{si} + \gamma_{sc} f_{co}^{'}A_{sc} + \gamma_{cc} f_{cc}^{'}A_{cc} \quad (22)$$

where A_{soe} denotes the effective area of the external steel tube considering local buckling effects; A_{si}, A_{sc} and A_{cc} represent the areas of internal steel tube, sandwiched concrete and core concrete, respectively; $f_{co}^{'}$ is the compressive cylinder strength of the sandwiched concrete; γ_{sc} and γ_{cc} represent the γ_c for the sandwiched concrete and core concrete, respectively; γ_{si} is the strength factor considering the effects of geometric imperfection, strain-hardening and hoop-tension on the inner tube and proposed by Liang and Fragomeni [39] as

$$\gamma_{si} = 1.458\left(\frac{D_i}{t_i}\right)^{-0.1} \qquad \left(0.9 \le \gamma_{si} \le 1.1\right) \quad (23)$$

To validate the design model proposed, the ultimate strengths of the tested columns presented in Table 1 were calculated using Eq. (22) and are compared with the experimental ultimate strengths in Table 3 and Fig. 22. The design model can predict average 97% of the experimental ultimate loads of the short columns. The standard deviation and coefficient of variation of the $P_{u,des} / P_{u,\exp}$ ratios are analyzed as 0.05.

The design model was used to investigate the effects of the diameter and thickness of the inner steel tube on the ultimate axial strengths of CFDST short columns. For this purpose, the ultimate axial loads of Columns C2-C8 where the inner steel tubes had various diameters and thicknesses as given in Table 2 were calculated using Eq. (22) and are compared with those predicted by the fiber element modeling technique in Table 4. It can be observed from Table 4 that increasing either the diameter or the thickness of the inner steel tube markedly increases the ultimate axial strengths of CFDST short columns. Excellent agreement between the design calculations and

numerical predictions is obtained. The mean $P_{u,des} / P_{u,num}$ of these columns is calculated as 0.98 with a coefficient variance of 0.02. The comparative studies demonstrate that the proposed simple design equation is capable of accurately computing the ultimate axial load of CFDST short columns under axial compression and can be used in the design of such composite columns in practice.

6. Comparisons with design codes

The experimental ultimate strengths of rectangular CFDST columns presented in Table 1 are further compared with the ultimate loads computed by the design methods provided in Eurocode 4 [5], ACI 318-11 [6], AISC 360-16 [7] and Japanese building code AIJ [8] given in Table 5. However, the current design codes do not cover the design of CFDST columns. Table 3 summarizes the code predictions and experimental ultimate load-carrying capacities. It is shown that the ACI 318-11 [6] and AISC 360-16 [7] design codes underestimate the column ultimate strengths remarkably due to neglecting the confinement to the core concrete provided by the inner circular tube. Eurocode 4 [5] and Japanese building code AIJ [8], which account for the confinement effects on the core concrete, generally overestimate the ultimate load-carrying capacities of CFDST short columns because these codes do not consider the local buckling effects of the outer square steel tube. The mean predicted-to-experimental ultimate strength by Eurocode 4 [5] and AIJ [8] was 1.06 and 1.01, respectively. The proposed design formula represented by Eq. (22) considers the local buckling of the outer steel tube and the confinement on the core concrete. It is seen that the design equation developed in the present study yields the best estimations of the ultimate loads of CFDST short columns.

7. Conclusions

This paper has presented a computationally efficient fiber-based computational model proposed for the inelastic modeling of rectangular thin-walled CFDST short columns with inner circular steel tube subjected to axial loading. The effects of the progressive local and post-local buckling of the external rectangular steel tube as well as the confinement on the core concrete within the internal circular steel tube have been taken into consideration in the theoretical model. A strength degradation factor for determining the concrete post-peak behavior has been proposed and incorporated in the material constitutive laws of concrete in CFDST columns. The comparisons of computer predictions with experimental data have demonstrated that the fiber-based simulation technology can accurately determine the responses of rectangular CFDST short columns. A design equation has been formulated for computing the ultimate axial strengths of rectangular CFDST short columns.

The conclusions drawn from the studies are:

(1) The inner circular steel tube remarkably increases the load-carrying capacity, ductility and the residual strength of rectangular short CFDST columns but does not affect the column initial stiffness notably. Increasing either the diameter or the thickness of the inner circular steel tube considerably increases the ultimate axial strengths of CFDST columns.

(2) The local buckling of the external steel tube may reduce the axial load capacity of CFDST short columns by about 7.9% and decrease the column residual strengths.

(3) The ultimate axial loads of CFDST columns are increased significantly by using higher strength sandwiched concrete, but the core concrete strength does not affect the column ultimate loads significantly.

(4) The ductility of CFDST short columns are decreased by using higher strength concrete.

(5) The axial load capacity of CFDST short columns is shown to increase with an increase in the yield stress of either the external or the internal steel tube.

(6) The B_o / D_o ratio of CFDST columns has a significant influence on the load-carrying capacity of CFDST columns.

(7) The methods given in Eurocode 4 [5] and AIJ [8] generally overestimate the ultimate axial loads of CFDST short column whereas the design approaches provided in ACI 318-11 [6] and AISC 360-16 [7] codes underestimate the ultimate strengths of CFDST short columns.

(8) The proposed design formula provides more accurate results of CFDST short columns than the design codes.

References

[1] Knowles RB, Park R. Strength of concrete filled steel columns. Journal of the Structural Division, ASCE 1969; 95 (12): 2565-2587.

[2] Tomii M, Yoshimura K, Morishita Y. Experimental studies on concrete-filled steel tubular stub columns under concentric loading. Proceeding of the international colloquium on stability of structures under static and dynamic loads, 1977; 718-741.

[3] Schneider SP. Axially loaded concrete-filled steel tubes. Journal of Structural Engineering, ASCE 1998; 124(10):1125-1138.

[4] Sakino K, Nakahara H, Morino S, Nishiyama I. Behavior of centrally loaded concrete-filled steel-tube short columns. Journal of Structural Engineering, ASCE 2004; 130 (2): 180-188.

[5] Eurocode 4. Design of composite steel and concrete structures-Part 1-1: general rules and rules for buildings. London, UK: British Standards Institution. EN 1994-1-1; 2004.

[6] ACI 318-11. Building code requirements for reinforced concrete. Detroit (MI). 2011.

[7] AISC 360-16. Specification for structural steel buildings. American Institute of Steel Construction. Chicago (IL); 2016.

[8] AIJ. Recommendations for design and construction of concrete filled steel tubular structures. Architectural Institute of Japan, Japan; 1997.

[9] Peng YY, Tan KF, Yao Y. Mechanical properties of duplex steel tube high- strength concrete short columns under axial compression. Journal of Wuhan University of Technology 2011; 33 (2): 105-109 (in Chinese).

[10] Hassanein MF, Kharoob OF, Liang QQ. Behaviour of circular concrete-filled lean duplex stainless steel–carbon steel tubular short columns. Engineering Structures 2013; 56: 83-94.

[11] Wan CY, Zha XX. Nonlinear analysis and design of concrete-filled dual steel tubular columns under axial loading. Steel and Composite Structures 2016; 20 (3): 571-597.

[12] Xiong MX, Xiong DX, Liew JR. Axial performance of short concrete filled steel tubes with high-and ultra-high-strength materials. Engineering Structures 2017; 136: 494-510.

[13] Ekmekyapar T, Al-Eliwi BJ. Concrete filled double circular steel tube (CFDCST) stub columns. Engineering Structures 2017; 135: 68-80.

[14] Ahmed M, Liang QQ, Patel VI, Hadi MNS. Numerical analysis of circular high strength concrete-filled double steel tubular short columns. Thin-Walled Structures 2018 (submitted).

[15] Hu HT, Huang CS, Wu MH, Wu YM. Nonlinear analysis of axially loaded concrete-filled tube columns with confinement effect. Journal of Structural Engineering, ASCE 2003; 129 (10): 1322-1329.

[16] Lu TQ, Zhao GF. Numerical method for analysis of ultimate strength of concrete-filled square steel tubular columns under eccentric compression reinforced by inner circular

steel tube. Journal of Dalian University of Technology 2001; 41 (5): 612-615 (in Chinese).

[17] Wang ZH, Cheng R. Axial bearing capacity of composite-sectioned square concrete-filled steel tube. Journal of Tsinghua University, Science and Technology 2005; 45 (12): 1596-1599 (in Chinese).

[18] Pei WJ. Research on mechanical performance of multibarrel tube-confined concrete columns. ME Thesis, Chang'an University, Xi'an, China, 2005 (in Chinese).

[19] Qian JR, Zhang Y, Ji XD, Cao WL. Test and analysis of axial compressive behavior of short composite-sectioned high strength concrete filled steel tubular columns. Journal of Building Structures 2011;32 (12): 162-169 (in Chinese).

[20] Wang Z-B, Tao Z, Yu Q. Axial compressive behaviour of concrete-filled double-tube stub columns with stiffeners. Thin-Walled Structures 2017; 120: 91-104.

[21] Liang QQ. Numerical simulation of high strength circular double-skin concrete-filled steel tubular slender columns. Engineering Structures 2018; 168: 205-217.

[22] Han LH, Huang H, Zhao XL. Analytical behavior of concrete-filled double skin steel tubular (CFDST) beam-columns under cyclic loading. Thin-Walled Structures 2009; 47: 668-680.

[23] Qian J, Li N, Ji X, Zhao Z. Experimental study on the seismic behavior of high strength concrete filled double-tube columns. Earthquake Engineering and Engineering Vibration 2014;13 (1): 47-57.

[24] Wang R, Han LH, Zhao XL, Rasmussen KJR. Analytical behavior of concrete filled double steel tubular (CFDST) members under lateral impact. Thin-Walled Structures 2016; 101: 129-140.

[25] Zhang FR, Wu CQ, Zhao XL, Heidarpour A, Li ZX. Experimental and numerical study of blast resistance of square CFDST columns with steel-fibre reinforced concrete. Engineering Structures 2017; 149: 50-63.

[26] Aghdamy A, Thambiratnam DP, Dhanasekar M, Saiedi S. Effects of load-related parameters on the response of concrete-filled double-skin steel tube columns subjected to lateral impact. Journal of Constructional Steel Research 2017; 138: 642-662.

[27] Ritchie C, Packer JA, Seica MV, Zhao XL. Flexural behavior of concrete-filled bouble-skin tubes subjected to blast loading. Journal of Structural Engineering, ASCE 2018; 144 (7): 04018076.

[28] Usami T. Effective width of locally buckled plates in compression and bending. Journal of Structural Engineering, ASCE 1993; 119 (5): 1358-1373.

[29] Uy B, Bradford MA. Local buckling of thin steel plates in composite construction: Experimental and theoretical study. Proceeding of the Institution of Civil Engineers, Structures and Buildings 1995; 110 (4): 426-40.

[30] Uy B. Strength of concrete filled steel box columns incorporating local buckling. Journal of Structural Engineering, ASCE 2000; 126 (3): 341-352.

[31] Liang QQ, Uy B. Theoretical study on the post-local buckling of steel plates in concrete-filled box columns. Computers & Structures 2000; 75 (5): 479-490.

[32] Liang QQ, Uy B, Liew JYR. Nonlinear analysis of concrete-filled thin-walled steel box columns with local buckling effects. Journal of Constructional Steel Research 2006; 62 (6): 581-591.

[33] Liang QQ, Uy B, Liew JYR. Local buckling of steel plates in concrete-filled thin-walled steel tubular beam–columns. Journal of Constructional Steel Research 2007; 63 (3): 396-405.

[34] Liang QQ. Performance-based analysis of concrete-filled steel tubular beam–columns, Part I: Theory and algorithms. Journal of Constructional Steel Research 2009; 65 (2): 363-372.

[35] Liang QQ. Performance-based analysis of concrete-filled steel tubular beam–columns, Part II: Verification and applications. Journal of Constructional Steel Research 2009; 65 (2): 351-362.

[36] Liang QQ. Nonlinear analysis of circular double-skin concrete-filled steel tubular columns under axial compression. Engineering Structures 2017; 131: 639-650.

[37] Patel VI, Liang QQ, Hadi MNS. Nonlinear analysis of concrete-filled steel tubular columns. Germany: Scholar's Press, 2015.

[38] Persson P-O, Strang G. A simple mesh generator in MATLAB. SIAM Review 2004; 46 (2): 329-345.

[39] Liang QQ, Fragomeni S. Nonlinear analysis of circular concrete-filled steel tubular short columns under axial loading. Journal of Constructional Steel Research 2009; 65 (12): 2186-2196.

[40] Mander JB. Seismic design of bridge piers. Ph.D. Thesis, Department of Civil Engineering, University of Canterbury, Christchurch, New Zealand; 1983.

[41] Susantha K, Ge H, Usami T. Uniaxial stress–strain relationship of concrete confined by various shaped steel tubes. Engineering Structures 2001; 23 (10): 1331-1347.

[42] Lai Z, Varma AH. Effective stress-strain relationships for analysis of noncompact and slender filled composite (CFT) members. Engineering Structures 2016; 124: 457-472.

[43] Katwal U, Tao Z, Hassan MK, Wang W-D. Simplified numerical modeling of axially loaded circular concrete-filled steel stub columns. Journal of Structural Engineering, ASCE 2017; 143 (12): 04017169.

[44] Lim JC, Ozbakkaloglu T. Stress–strain model for normal-and light-weight concretes under uniaxial and triaxial compression. Construction and Building Materials 2014; 71: 492-509.

[45] Mander JB, Priestley MJ, Park R. Theoretical stress-strain model for confined concrete. Journal of Structural Engineering, ASCE 1988; 114 (8): 1804-1826.

[46] Tang J, Hino S, Kuroda I, Ohta T. Modeling of stress-strain relationships for steel and concrete in concrete filled circular steel tubular columns. Steel Construction Engineering, JSSC 1996; 3 (11): 35-46.

[47] Oehlers DJ, Bradford MA. Elementary behavior of composite steel and concrete structural members. Oxford U.K.: Butterworth-Heinemann, 1999.

Figures and tables

Table 1 Comparison of predicted and experimental ultimate axial loads of square CFDST short columns.

Specimen	Outer Tube			Inner Tube			Concrete		Ultimate axial load			Ref.
	$B_o \times D_o \times t_o$ (mm)	$\frac{D_o}{t_o}$	f_{syo} (MPa)	$D_i \times t_i$ (mm)	$\frac{D_i}{t_i}$	f_{syi} (MPa)	f'_{co} (MPa)	f'_{ci} (MPa)	$P_{u,\exp}$ (kN)	$P_{u,num}$ (kN)	$\frac{P_{u,num}}{P_{u,\exp}}$	
I-CSCFT1	180×180×3.62	49.7	348	89×2.6	34.2	314	89.85	74.38	3643	3436	0.94	[19]
I-CSCFT2	180×180×3.62	49.7	348	89×3.32	26.8	324	89.85	74.38	3583	3487	0.97	
I-CSCFT4	180×180×3.62	49.7	348	114×4.56	25.0	322	89.85	74.38	3820	3707	0.97	
I-CSCFT5	180×180×3.62	49.7	348	140×2.84	49.3	345	89.85	74.38	3940	3541	0.90	
I-CSCFT7	180×180×5.4	33.3	338	89×2.6	34.2	314	89.85	74.38	3865	3784	0.98	
I-CSCFT8	180×180×5.4	33.3	338	89×3.32	26.8	324	89.85	74.38	3947	3836	0.97	
I-CSCFT9	180×180×5.4	33.3	338	114×3.35	34.0	328	89.85	74.38	4045	3976	0.98	
I-CSCFT10	180×180×5.4	33.3	338	114×4.56	25.0	322	89.85	74.38	4121	4063	0.99	
I-CSCFT11	180×180×5.4	33.3	338	140×2.84	49.3	345	89.85	74.38	4251	3874	0.91	
I-CSCFT12	180×180×5.4	33.3	338	140×3.97	35.3	308	89.85	74.38	4258	4147	0.97	
II-CSCFT1	180×180×3.62	49.7	348	89×2.6	34.2	314	74.38	89.85	3355	3186	0.95	
II-CSCFT2	180×180×3.62	49.7	348	114×3.35	34.0	328	74.38	89.85	3686	3493	0.95	
II-CSCFT4	180×180×5.4	33.3	338	89×2.6	34.2	314	74.38	89.85	3814	3553	0.93	
II-CSCFT5	180×180×5.4	33.3	338	114×3.35	34.0	328	74.38	89.85	4043	3867	0.96	
II-CSCFT6	180×180×5.4	33.3	338	140×3.97	35.3	308	74.38	89.85	4428	4172	0.94	
II-CSCFT7	180×180×5.4	33.3	338	89×3.32	26.8	324	74.38	89.85	3855	3601	0.93	
III-CSCFT1	180×180×3.62	49.7	348	89×2.6	34.2	314	74.38	74.38	3198	3096	0.97	
III-CSCFT2	180×180×3.62	49.7	348	114×3.35	34.0	328	74.38	74.38	3415	3343	0.98	
III-CSCFT3	180×180×3.62	49.7	348	140×3.97	35.3	308	74.38	74.38	4120	3588	0.87	
III-CSCFT4	180×180×5.4	33.3	338	89×2.6	34.2	314	74.38	74.38	4021	3463	0.86	
III-CSCFT5	180×180×5.4	33.3	338	114×3.35	34.0	328	74.38	74.38	4165	3716	0.89	
III-CSCFT6	180×180×5.4	33.3	338	140×3.97	35.3	308	74.38	74.38	4436	3965	0.89	
III-CSCFT7	180×180×5.4	33.3	338	89×3.32	26.8	324	74.38	74.38	3900	3515	0.90	
SDS1-40a	200×200×2.01	99.5	230	136.5×1.94	70.4	492.1	43.44	43.44	2450	2379	0.97	[20]
SDS1-40b	200×200×2.01	99.5	230	136.5×1.94	70.4	492.1	43.44	43.44	2383	2379	1.00	
SDS1-70a	200×200×2.01	99.5	230	136.5×1.94	70.4	492.1	43.44	67.83	2997	2728	0.91	
SDS1-70b	200×200×2.01	99.5	230	136.5×1.94	70.4	492.1	43.44	67.83	2806	2728	0.97	
SDS2-40a	200×200×2.01	99.5	230	114.6×3.93	29.2	377.1	43.44	43.44	2366	2429	1.03	
SDS2-40b	200×200×2.01	99.5	230	114.6×3.93	29.2	377.1	43.44	43.44	2463	2429	0.99	
SDS2-70a	200×200×2.01	99.5	230	114.6×3.93	29.2	377.1	43.44	67.83	2765	2659	0.96	
SDS2-70b	200×200×2.01	99.5	230	114.6×3.93	29.2	377.1	43.44	67.83	2884	2659	0.92	
SDS3-40a	200×200×2.01	99.5	230	140.1×3.78	37.1	322.4	43.44	43.44	2505	2502	1.00	
SDS3-40b	200×200×2.01	99.5	230	140.1×3.78	37.1	322.4	43.44	43.44	2479	2502	1.01	
SDS3-70a	200×200×2.01	99.5	230	140.1×3.78	37.1	322.4	43.44	67.83	3144	2881	0.92	
SDS3-70b	200×200×2.01	99.5	230	140.1×3.78	37.1	322.4	43.44	67.83	3100	2881	0.93	
G1-2	120×120×2.6	46.2	407.5	58.5×1.4	41.8	352.5	29.92	29.92	980	946	0.97	[18]
G1-3	120×120×2.6	46.2	407.5	74×0.9	82.2	680	29.92	29.92	1040	1013	0.97	
G1-4	120×120×2.6	46.2	407.5	83×0.9	92.2	597	29.92	29.92	1080	1019	0.94	
Mean											0.95	
Standard Deviation (SD)											0.04	
Coefficients of Variance (COV)											0.04	

Table 2 Geometric and material properties of CFDST short columns used in the parameter study.

Column	Outer Tube			Inner Tube			Concrete	
	$B_o \times D_o \times t_o$ (mm)	D_o / t_o	f_{syc} (MPa)	$D_i \times t_i$ (mm)	D_i / t_i	f_{syi} (MPa)	f_{co} (MPa)	f_{ci} (MPa)
C1	450×450×12.8	35.2	350	-	-	-	-	70
C2	450×450×7.5	60	350	300×10	30	350	70	70
C3	450×450×7.5	60	350	150×10	15	350	70	70
C4	450×450×7.5	60	350	200×10	20	350	70	70
C5	450×450×7.5	60	350	250×10	25	350	70	70
C6	450×450×7.5	60	350	300×6.0	50	350	70	70
C7	450×450×7.5	60	350	300×7.5	40	350	70	70
C8	450×450×7.5	60	350	300×15	20	350	70	70
C9	200×200×2.01	99.5	492	136.5×1.94	70.4	492	35	35
C10	650×650×10	65	350	350×10	35	350	35	35
C11	650×650×10	65	350	350×10	35	350	50	50
C12	650×650×10	65	350	350×10	35	350	70	70
C13	650×650×10	65	350	350×10	35	350	90	90
C14	650×650×10	65	350	350×10	35	350	50	35
C15	650×650×10	65	350	350×10	35	350	50	50
C16	650×650×10	65	350	350×10	35	350	50	70
C17	650×650×10	65	350	350×10	35	350	50	90
C18	650×650×10	65	350	350×10	35	350	35	50
C19	650×650×10	65	350	350×10	35	350	50	50
C20	650×650×10	65	350	350×10	35	350	70	50
C21	650×650×10	65	350	350×10	35	350	90	50
C22	450×450×7.5	60	250	300×10	30	350	70	70
C23	450×450×7.5	60	350	300×10	30	350	70	70
C24	450×450×7.5	60	450	300×10	30	350	70	70
C25	450×450×7.5	60	520	300×10	30	350	70	70
C26	450×450×7.5	60	350	300×10	30	250	70	70
C27	450×450×7.5	60	350	300×10	30	350	70	70
C28	450×450×7.5	60	350	300×10	30	450	70	70
C29	450×450×7.5	60	350	300×10	30	520	70	70
C30	400×800×12	66.67	450	350×10	35	450	90	90
C31	600×800×12	66.67	450	350×10	35	450	90	90
C32	1000×800×12	66.67	450	350×10	35	450	90	90
C33	1200×800×12	66.67	450	350×10	35	450	90	90

Table 3 Comparison of ultimate strengths of rectangular CFDST short columns with the code predictions.

Specimen	$P_{u,\exp}$ (kN)	$P_{u,EC4}$ (kN)	$P_{u,ACi}$ (kN)	$P_{u,AISC}$ (kN)	$P_{u,AIJ}$ (kN)	$P_{u,des}$ (kN)	$\frac{P_{u,EC4}}{P_{u,\exp}}$	$\frac{P_{u,ACI}}{P_{u,\exp}}$	$\frac{P_{u,AISC}}{P_{u,\exp}}$	$\frac{P_{u,AIJ}}{P_{u,\exp}}$	$\frac{P_{u,des}}{P_{u,\exp}}$
I-CSCFT1	3643	3765	3263	3280	3703	3525	1.03	0.90	0.90	1.02	0.97
I-CSCFT2	3583	3852	3319	3334	3775	3599	1.08	0.93	0.93	1.05	1.00
I-CSCFT4	3820	4072	3440	3479	3937	3855	1.07	0.90	0.91	1.03	1.01
I-CSCFT5	3940	3911	3310	3392	3777	3541	0.99	0.84	0.86	0.96	0.90
I-CSCFT7	3865	4049	3556	3574	3980	3844	1.05	0.92	0.92	1.03	0.99
I-CSCFT8	3947	4138	3612	3628	4052	3917	1.05	0.92	0.92	1.03	0.99
I-CSCFT9	4045	4209	3635	3678	4087	4059	1.04	0.90	0.91	1.01	1.00
I-CSCFT10	4121	4364	3733	3772	4213	4173	1.06	0.91	0.92	1.02	1.01
I-CSCFT11	4251	4200	3603	3685	4054	3858	0.99	0.85	0.87	0.95	0.91
I-CSCFT12	4258	4321	3674	3752	4146	4199	1.01	0.86	0.88	0.97	0.99
II-CSCFT1	3355	3489	3025	3053	3423	3263	1.04	0.90	0.91	1.02	0.97
II-CSCFT2	3686	3760	3203	3261	3647	3588	1.02	0.87	0.88	0.99	0.97
II-CSCFT4	3814	3791	3334	3362	3718	3598	0.99	0.87	0.88	0.97	0.94
II-CSCFT5	4043	4067	3512	3570	3942	3923	1.01	0.87	0.88	0.98	0.97
II-CSCFT6	4428	4330	3680	3779	4153	4184	0.98	0.83	0.85	0.94	0.94
II-CSCFT7	3855	3879	3388	3414	3788	3662	1.01	0.88	0.89	0.98	0.95
III-CSCFT1	3198	3405	2953	2973	3338	3188	1.06	0.92	0.93	1.04	1.00
III-CSCFT2	3415	3625	3084	3130	3507	3461	1.06	0.90	0.92	1.03	1.01
III-CSCFT3	4120	3817	3191	3271	3646	3676	0.93	0.77	0.79	0.88	0.89
III-CSCFT4	4021	3709	3262	3283	3633	3524	0.92	0.81	0.82	0.90	0.88
III-CSCFT5	4165	3933	3393	3439	3802	3795	0.94	0.81	0.83	0.91	0.91
III-CSCFT6	4436	4126	3500	3580	3941	4010	0.93	0.79	0.81	0.89	0.90
III-CSCFT7	3900	3798	3318	3337	3705	3597	0.97	0.85	0.86	0.95	0.92
SDS1-40a	2450	2738	2235	2281	2589	2379	1.12	0.91	0.93	1.06	0.94
SDS1-40b	2383	2738	2235	2281	2589	2379	1.15	0.94	0.96	1.09	0.97
SDS1-70a	2997	3064	2522	2597	2926	2728	1.02	0.84	0.87	0.98	0.88
SDS1-70b	2806	3064	2522	2597	2926	2728	1.09	0.90	0.93	1.04	0.95
SDS2-40a	2366	2875	2327	2351	2707	2429	1.22	0.98	0.99	1.14	1.08
SDS2-40b	2463	2875	2327	2351	2707	2429	1.17	0.94	0.95	1.10	1.04
SDS2-70a	2765	3084	2512	2555	2925	2659	1.12	0.91	0.92	1.06	1.03
SDS2-70b	2884	3084	2512	2555	2925	2659	1.07	0.87	0.89	1.01	0.99
SDS3-40a	2505	2889	2324	2370	2705	2502	1.15	0.93	0.95	1.08	1.04
SDS3-40b	2479	2889	2324	2370	2705	2502	1.17	0.94	0.96	1.09	1.05
SDS3-70a	3144	3212	2610	2685	3041	2881	1.02	0.83	0.85	0.97	0.96
SDS3-70b	3100	3212	2610	2685	3041	2881	1.04	0.84	0.87	0.98	0.97
G1-2	980	1031	915	917	997	944	1.05	0.93	0.94	1.02	0.96
G1-3	1040	1124	969	976	1065	998	1.08	0.93	0.94	1.02	0.96
G1-4	1080	1122	968	978	1063	997	1.04	0.90	0.91	0.98	0.92
Mean							1.06	0.88	0.90	1.01	0.97
Standard Deviation (SD)							0.09	0.06	0.06	0.07	0.05
Coefficients of Variance (COV)							0.09	0.07	0.06	0.07	0.05

Table 4 Comparison of design ultimate strengths of CFDST columns with numerical predictions.

Column	$P_{u,des}$ (kN)	$P_{u,num}$ (kN)	$\frac{P_{u,des}}{P_{u,num}}$
C2	19376	19461	1.00
C3	16393	16894	0.97
C4	17368	17621	0.99
C5	18367	18462	0.99
C6	16835	17726	0.95
C7	18462	18787	0.98
C8	20897	20650	1.01
Mean			0.98
Standard Deviation (SD)			0.02
Coefficients of Variance (COV)			0.02

Table 5 Strength prediction formulas for rectangular CFDST short columns by design codes.

Design codes	Design equations
Eurocode 4 [5]	Circular CFST columns: $P_u = \eta_a A_s f_{sy} + A_c f_c (1 + \eta_c \frac{t}{D} \frac{f_{sy}}{f_c})$ $\eta_a = 0.25(3 + 2\bar{\lambda}) \qquad (\eta_a \le 1.0)$ $\eta_c = 4.9 - 18.5\bar{\lambda} + 17\bar{\lambda}^2 \quad (\eta_c > 0)$ where the relative slenderness ratio is $\bar{\lambda} = \sqrt{\frac{N_{pl,Rk}}{N_{cr}}}$ Rectangular CFST columns: $P_u = A_s f_{sy} + A_c f_c'$ Rectangular CFDST columns with inner circular tube: $P_{u,EC4} = A_{so} f_{syo} + A_{sc} f_c' + \eta_a A_{si} f_{syi} + A_{cc} f_{cc} (1 + \eta_c \frac{t_i}{d_i} \frac{f_{syi}}{f_{ci}})$
ACI 318-11 [6]	$P_{u,ACI} = A_{so} f_{syo} + 0.85 A_{sc} f_{sc} + A_{si} f_{syi} + 0.85 A_{cc} f_{cc}$
AISC 360-16 [7]	$P_{u,AISC} = \begin{cases} P_o \left[0.658^{(P_o/P_e)}\right] & \text{for } P_e \ge 0.44 P_o \\ 0.877 P_e & \text{for } P_e < 0.44 P_o \end{cases}$ $P_o = A_{so} f_{syo} + C_2 A_{sc} f_{sc} + A_{si} f_{syi} + C_2 A_{cc} f_{cc}$ $P_e = \frac{\pi^2}{(KL)^2} (EI)_{eff}$ $(EI)_{eff} = E_{so} I_{so} + E_{si} I_{si} + C_4 E_{sc} I_{sc} + C_4 E_{cc} I_{cc}$ $C_4 = 0.6 + 2\left(\frac{A_s}{A_s + A_c}\right) \le 0.9$ $C_2 = \begin{cases} 0.95 & \text{for circular cross-section} \\ 0.85 & \text{for rectangular cross-section} \end{cases}$
AIJ [8]	$P_{u,AIJ} = A_{sc} f_{sc} + (1+\eta) A_{so} f_{syo} + + A_{cc} f_{cc} + (1+\eta) A_{si} f_{syi}$ $\eta = \begin{cases} 0.27 & \text{for circular cross-section} \\ 0 & \text{for rectangular cross-section} \end{cases}$

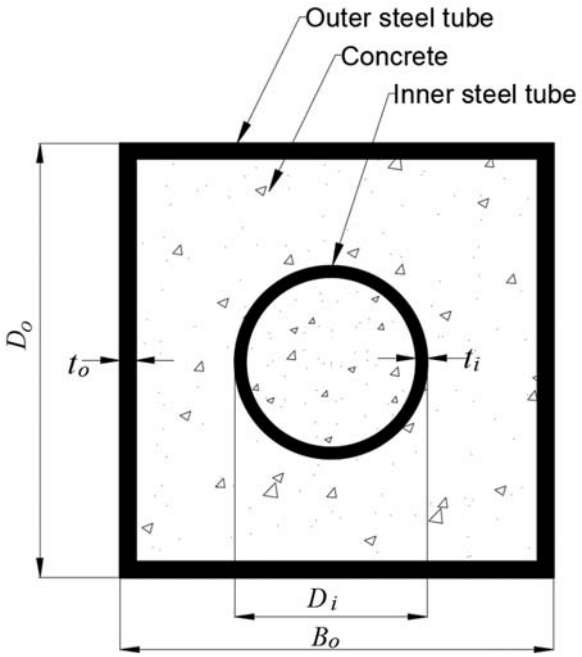

Fig. 1. Cross-section of rectangular CFDST column with inner circular steel tube.

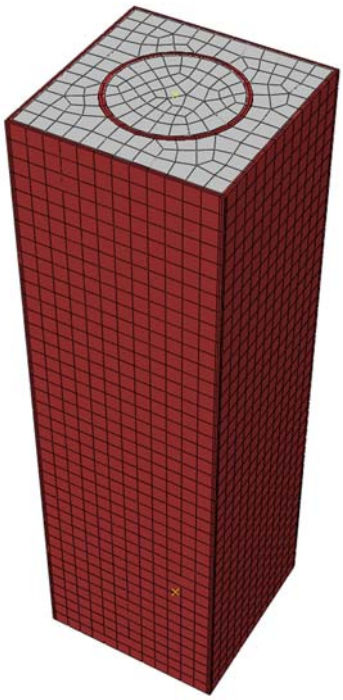

Fig. 2. Finite element model of CFDST column.

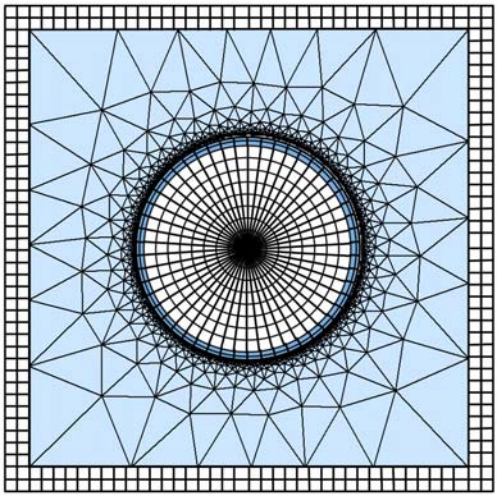

Fig. 3. Typical fiber mesh in CFDST column section with inner circular steel tube.

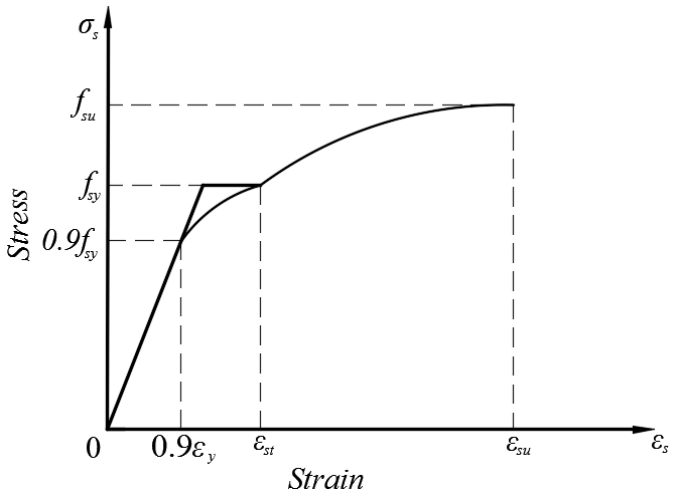

Fig. 4. Stress-strain curve for structural steel.

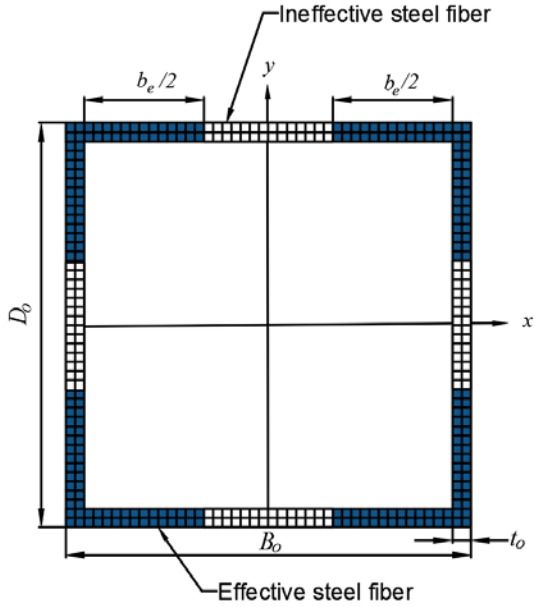

Fig. 5. Effective width of the outer rectangular steel tube.

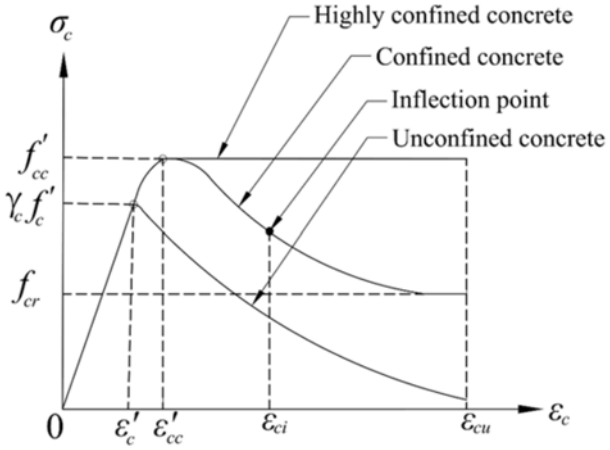

Fig. 6. Stress-strain curves for confined concrete in rectangular CFDST column.

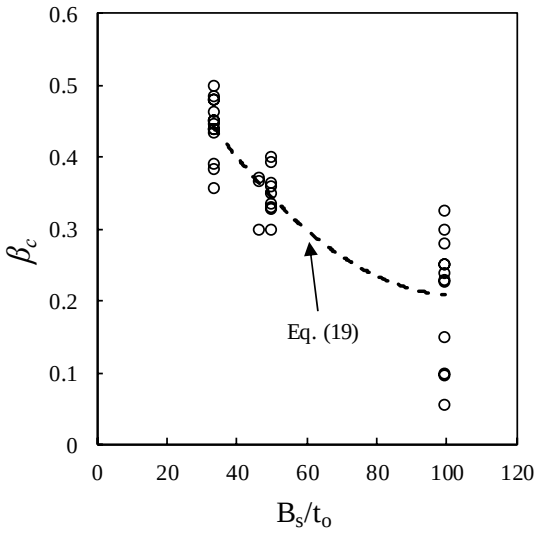

Fig. 7. Verification of the proposed expression for β_c .

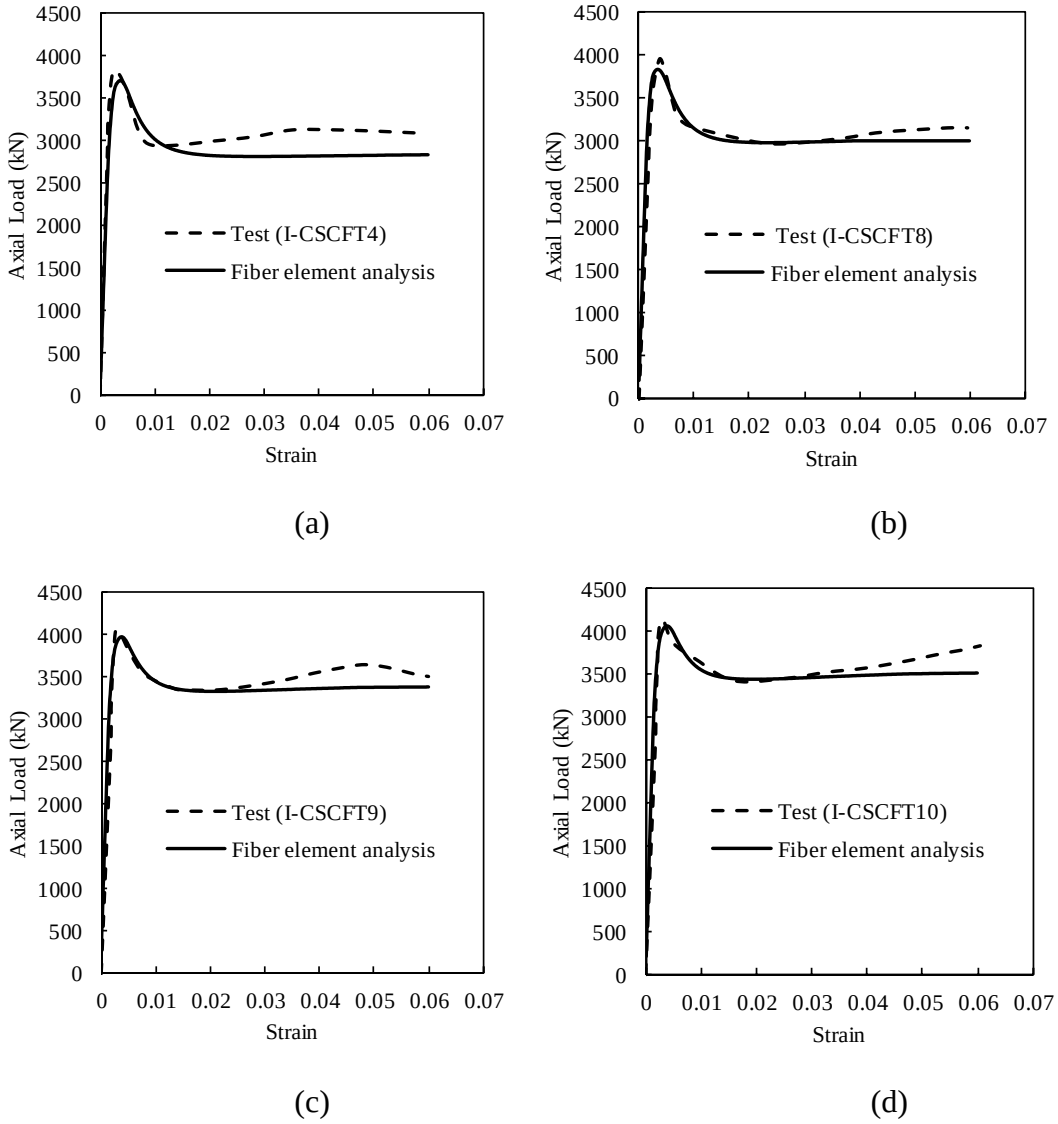

Fig. 8. Comparison of predicted and experimental axial load-strain curves of CFDST short columns tested by Qian et al. [19].

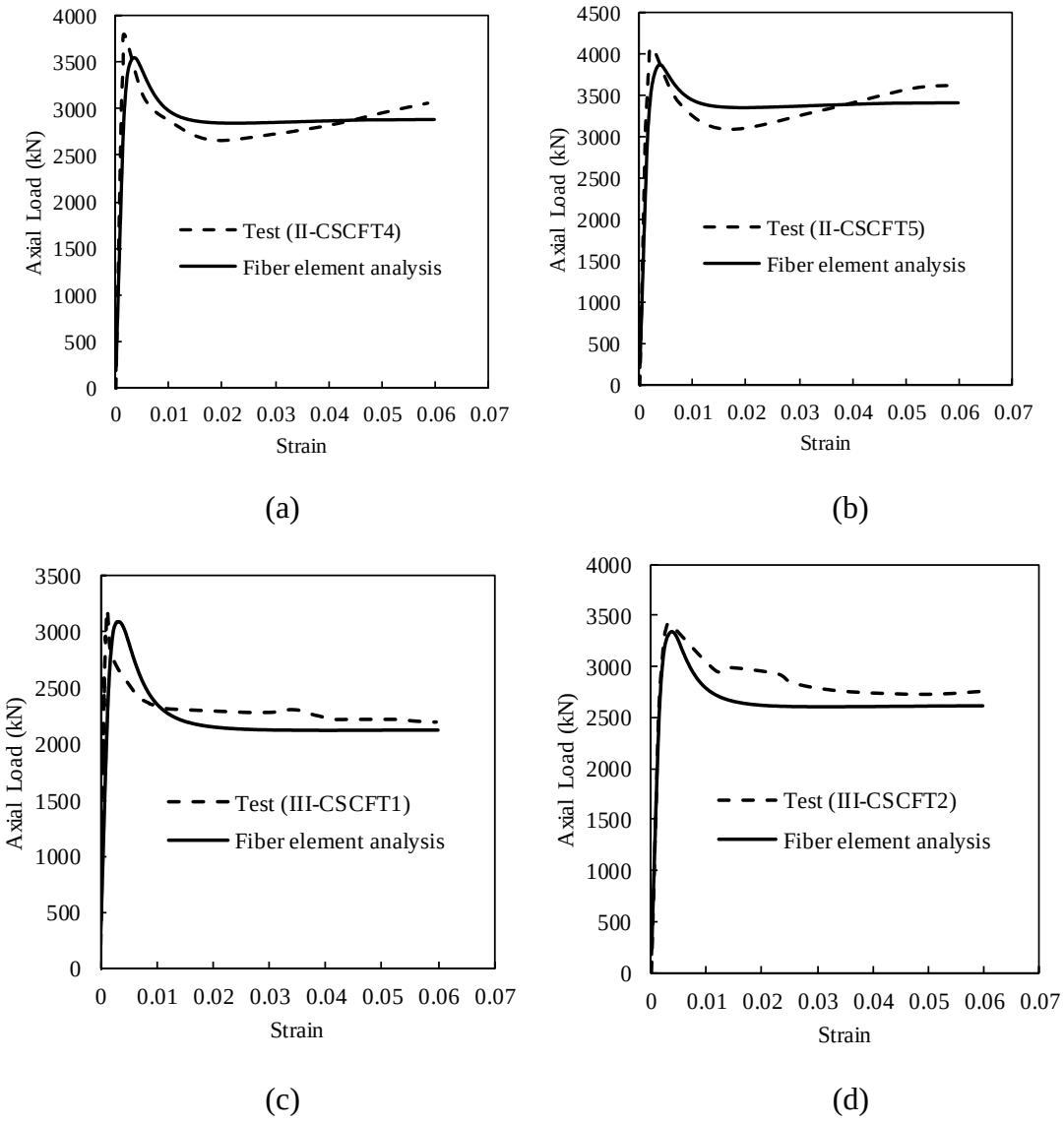

Fig. 9. Comparison of predicted and experimental axial load-strain curves of CFDST columns tested by Qian et al. [19].

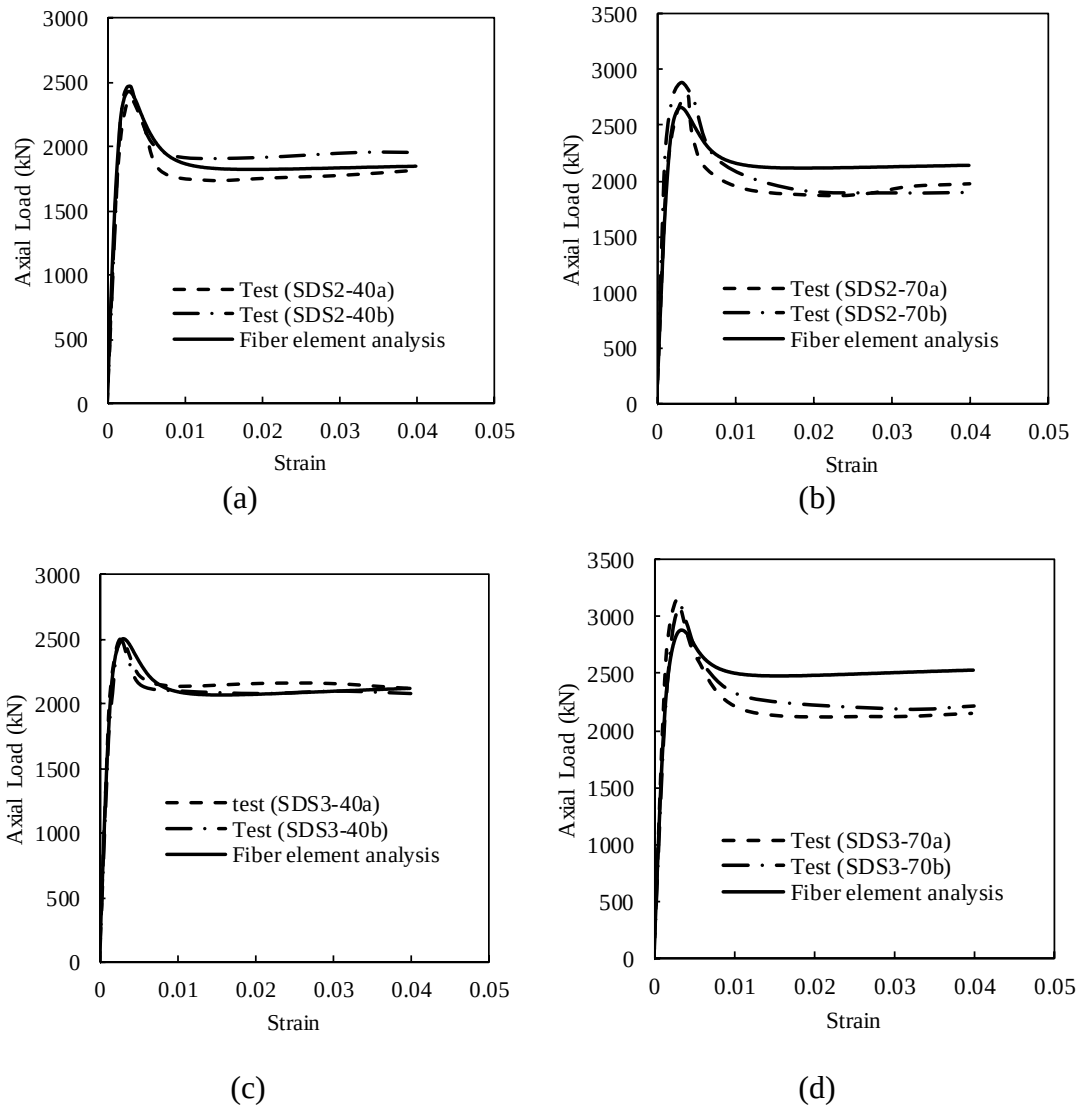

Fig. 10. Comparison of predicted and experimental axial load-strain curves of CFDST columns tested by Wang et al. [20].

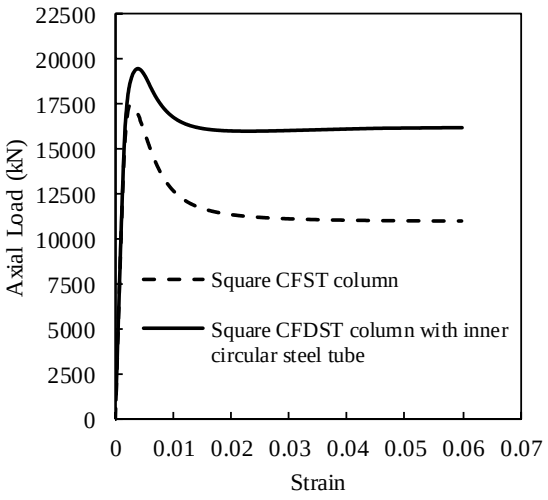

Fig. 11. Effects of the inner steel tube on the axial load-strain responses of CFDST short column.

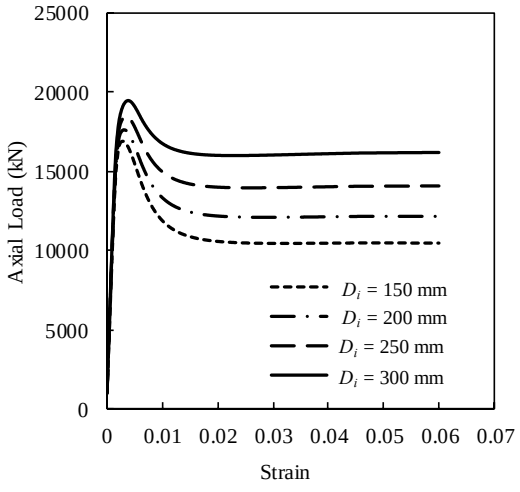

Fig. 12. Effects of the diameter of the inner steel tube on the axial load-strain responses of CFDST short columns.

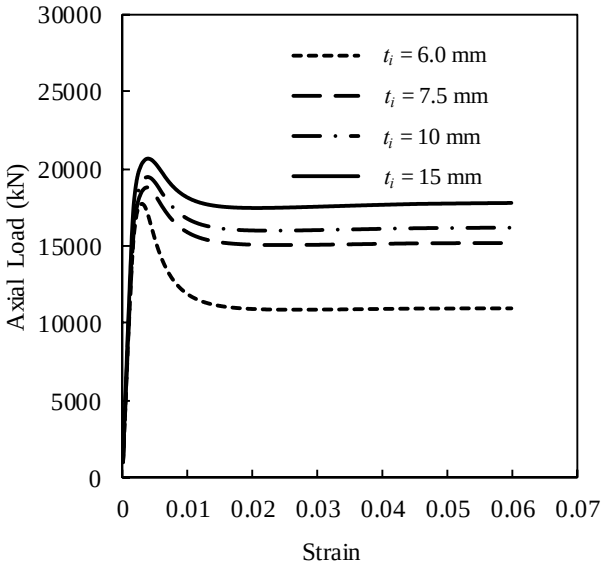

Fig. 13. Effects of the thickness of the inner steel tube on the axial load-strain responses of CFDST short columns.

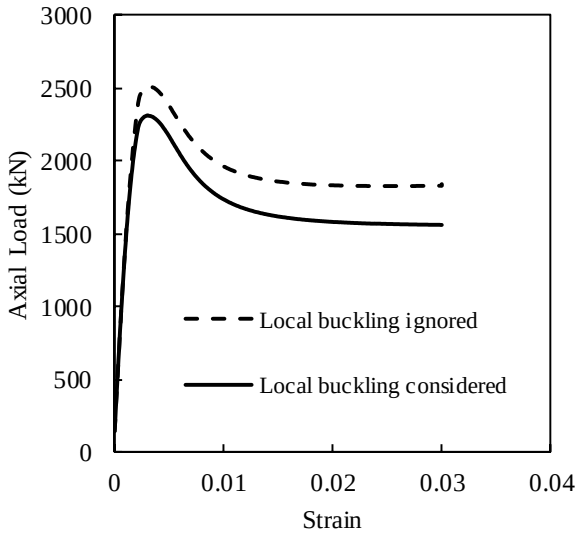

Fig. 14. Effects of local buckling of the outer steel tube on the axial load-strain responses of CFDST short columns.

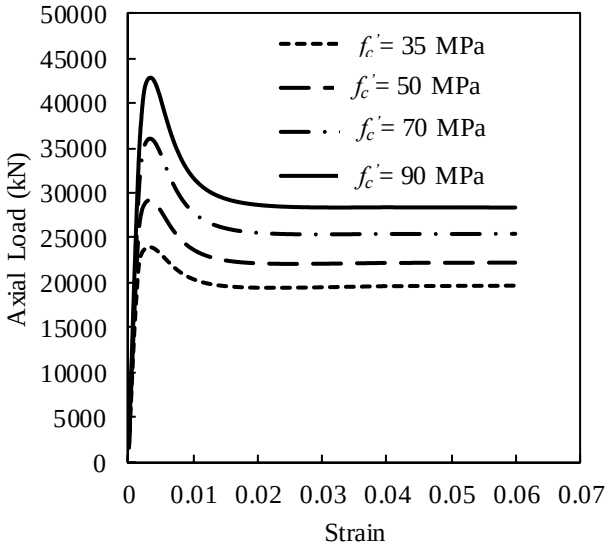

Fig. 15. Effects of concrete compressive strength on the axial load-strain responses of CFDST short columns.

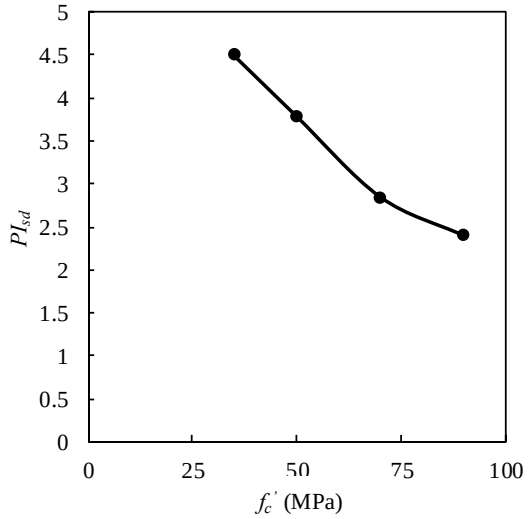

Fig. 16. Strain ductility indices of CFDST short columns with various concrete strengths.

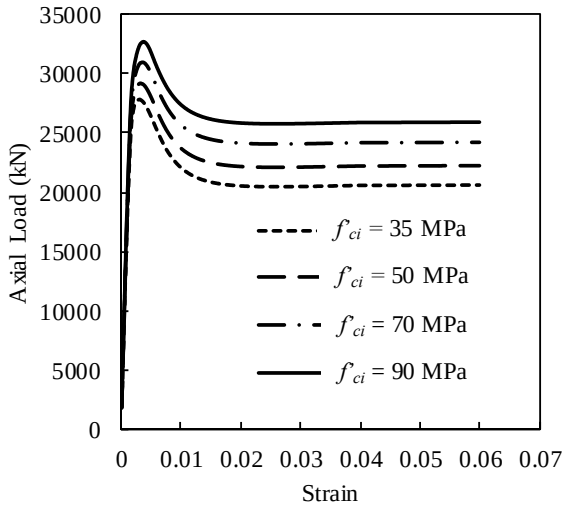

Fig. 17. Effects of core concrete compressive strength on the axial load-strain response of CFDST columns.

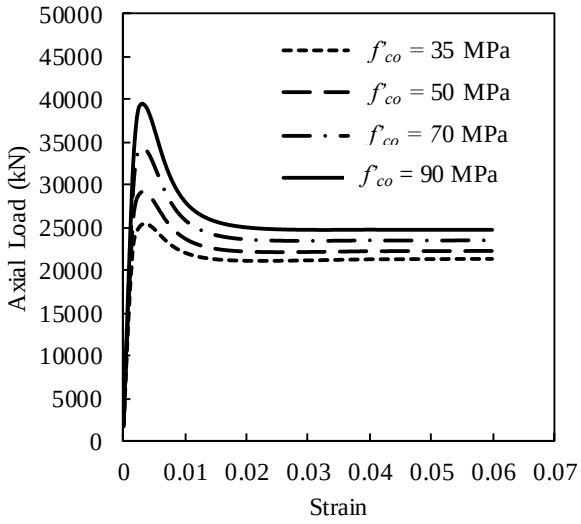

Fig. 18. Effects of sandwiched concrete compressive strength on the axial load-strain responses of CFDST columns.

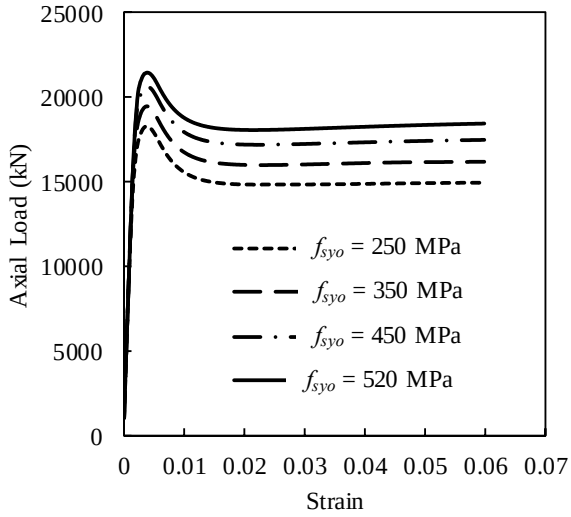

Fig. 19. Effects of the yield strength of the outer steel tube on the axial load-strain responses of CFDST short columns.

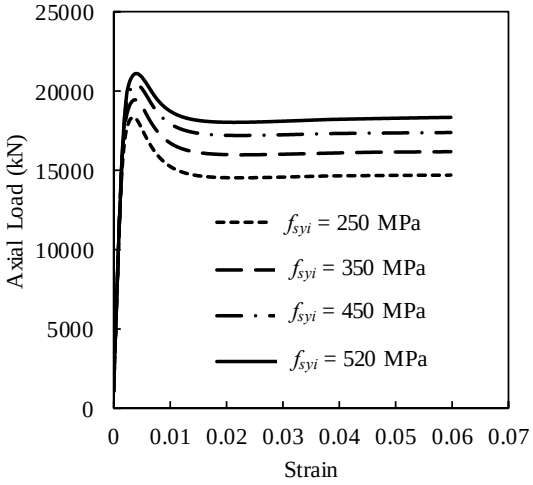

Fig. 20. Effects of the yield strength of the inner steel tube on the axial load-strain responses of CFDST short columns.

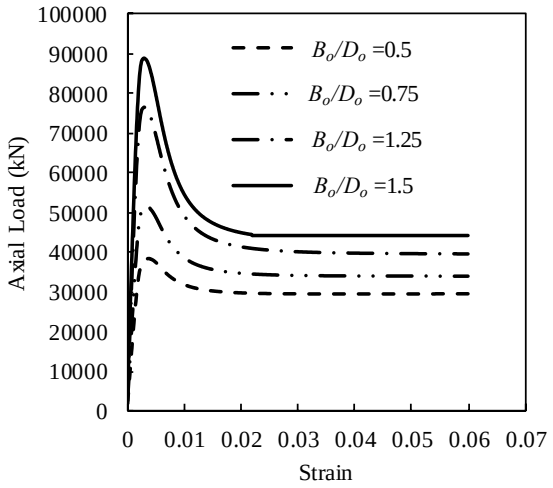

Fig. 21. Effects of the width-to-depth ratios on the axial load-strain responses of CFDST short columns.

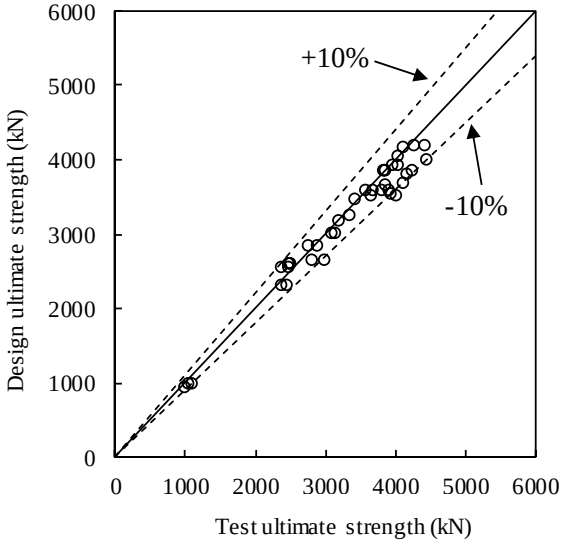

Fig. 22. Verification of the design model.